AGU PUBLICATIONS

Geophysical Research Letters

RESEARCH LETTER
10.1002/2017GL076822

Key Points:
- GWO phase explains significant variability in U.S. severe hail frequency
- Damaging hailstones are most frequent in GWO phases 1, 2, 3, and 8
- Observed hail report variability is corroborated by GWO modulated favorable atmospheric environments

Correspondence to:
V. A. Gensini,
vgensini@niu.edu

Citation:
Gensini, V. A., & Allen, J. T. (2018). U.S. hail frequency and the Global Wind Oscillation. *Geophysical Research Letters*, *45*. https://doi.org/10.1002/2017GL076822

Received 20 NOV 2017
Accepted 19 JAN 2018
Accepted article online 29 JAN 2018

U.S. Hail Frequency and the Global Wind Oscillation

Vittorio A. Gensini[1] **and John T. Allen**[2]

[1]Department of Geographic and Atmospheric Sciences, Northern Illinois University, DeKalb, IL, USA, [2]Department of Earth and Atmospheric Sciences, Central Michigan University, Mount Pleasant, MI, USA

Abstract Changes in Earth relative atmospheric angular momentum can be described by an index known as the Global Wind Oscillation. This global index accounts for changes in Earth's atmospheric budget of relative angular momentum through interactions of tropical convection anomalies, extratropical dynamics, and engagement of surface torques (e.g., friction and mountain). It is shown herein that U.S. hail events are more (less) likely to occur in low (high) atmospheric angular momentum base states when excluding weak Global Wind Oscillation days, with the strongest relationships found in the boreal spring and fall. Severe, significant severe, and giant hail events are more likely to occur during Global Wind Oscillation phases 8, 1, 2, and 3 during the peak of U.S. severe weather season. Lower frequencies of hail events are generally found in Global Wind Oscillation phases 4–7 but vary based on Global Wind Oscillation amplitude and month. In addition, probabilistic anomalies of atmospheric ingredients supportive of hail producing supercell thunderstorms closely mimic locations of reported hail frequency, helping to corroborate report results.

Plain Language Summary Changes in patterns of wind across Earth have been demonstrated to impact the likelihood of weather patterns conducive to severe weather. This research shows that jet stream wind patterns that are wavy (meridional) are more likely to produce severe hailstorms. In addition, we demonstrate a framework that may be useful for the advanced prediction of damaging hailstones that are mostly likely to cause economic loss.

1. Introduction

Relationships between the climate system and U.S. severe thunderstorm variability for the boreal spring have previously been identified for several atmospheric and oceanic features. These teleconnections include the Madden-Julian Oscillation (MJO; (Barrett & Gensini, 2013; Barrett & Henley, 2015; Thompson & Roundy, 2012), El Niño–Southern Oscillation (Allen et al., 2015; Cook & Schaefer, 2008; Cook et al., 2017; Lee et al., 2012, 2016), and sea surface temperatures in the Gulf of Mexico (Jung & Kirtman, 2016; Molina et al., 2016). The dynamical mechanisms of these teleconnections on U.S. severe thunderstorms focus on the modulation of the subtropical or polar jet stream position via enhancement or suppression of the baroclinic gradient by tropical convection in the east central Pacific Ocean (Allen et al., 2015; Cook et al., 2017), tropical convection modulating downstream Rossby waves (Barrett & Gensini, 2013; Barrett & Henley, 2015; Thompson & Roundy, 2012), and potential for a rich source region of anomalous surface water vapor mixing ratios related to Gulf of Mexico sea surface temperatures (Molina et al., 2016). Periodicity of these teleconnections ranges from subseasonal to seasonal time scales (i.e., 2 weeks to beyond 2 months), and distinguishing among leading modes of variability relies on a thorough comprehension of the interplay among various oceanic and atmospheric dynamical processes.

Unlike the aforementioned metrics, the Global Wind Oscillation (GWO; Weickmann & Berry, 2007, 2009) is a holistic description of changes in global relative atmospheric angular momentum (AAM) budget, including signals projected onto the atmosphere by various teleconnection modes. Previous research has indicated a relationship between the GWO and U.S. tornado frequency (Gensini & Marinaro, 2015; Moore, 2017). Since a majority of tornadoes are produced by supercell thunderstorms, it follows that variability in large hail frequency may also be explained by this metric, as large hail events are often an additional by-product (Allen et al., 2015; Blair et al., 2017). Unlike tornadoes, few studies have considered the influence teleconnections on the frequency variability of damaging hailstones (Allen et al., 2015; Barrett & Henley, 2015; Lepore et al., 2017).

Hail reflects the most economically damaging of the hazards posed by severe thunderstorms, producing roughly 60% of the annual average $11.23 billion losses in the United States (Gunturi & Tippett, 2017), compared to 20% for both damaging wind and tornadoes. Hailstorms are relatively common over the continental United States, with several climatologies derived from observations (Allen & Tippett, 2015; Allen et al., 2017; Changnon, 1977; Changnon & Changnon, 2000; Doswell et al., 2005; Kelly et al., 1985), remotely sensed proxy observations (Cecil & Blankenship, 2012; Cintineo et al., 2012), and environmental proxies for hail occurrence (Allen et al., 2015). One parameter capable of identifying these storms is the supercell composite parameter (SCP; Thompson et al., 2003), which combines 0–6 km vertical wind shear (S06; m s^{-1}), 0–3 km storm relative helicity (m^2 s^{-2}), and surface-based convective available potential energy (J kg^{-1}) into one convenient index that is skillful at statistically discriminating between supercell and nonsupercell environments. Supercells produce the vast majority of hailstones in excess of 5 cm in diameter (Blair et al., 2017), suggesting that such a proxy would be a useful metric for identifying favorable severe hail environments.

This paper explores the influence of the GWO on hail frequency and intensity over the United States. Hail intensity is assessed using three categories of hail diameter observations: severe hail (SEV; ≥2.5 cm), significant severe hail (SIG; ≥5 cm), and giant hail (GIANT; ≥10 cm). Finally, we relate hail report variability by GWO phase to the environmental SCP to assess confidence of the hail report relationships.

2. Data and Approach

2.1. Hail Observations

Hail observations were obtained from the National Centers for Environmental Information Storm Data (Schaefer & Edwards, 1999) for the period 1979–2016. Data were aggregated to "hail days," in which any day with at least one U.S. hail report was counted. These data were further stratified into SIG hail and GIANT hail days. Hail observations are sensitive to significant spatial and nonmeteorological biases relating to spatial variations in population, hail size being estimated rather than measured, and other discontinuities in the record (Allen & Tippett, 2015). Climatologically speaking, such errors are much less likely influence the stratified results herein given the large sample sizes. Despite the advantages that this large sample provides, there are observed trends in hail observations through time, and thus, the assessment of interannual variability in the report signal is avoided (Allen & Tippett, 2015).

2.2. Global Wind Oscillation

Data from the National Center for Atmospheric Research/Department of Energy reanalysis 2 project (R2; Computational and Information Systems Laboratory, 2000; Kalnay et al., 1996) was used on the native National Center for Atmospheric Research T62 Gaussian grid to calculate the GWO (28 vertical levels using σ coordinates). In order to compute the GWO, one needs to first compute standardized anomalies of AAM, then its tendency. AAM was calculated using daily averages of zonal wind from R2 for the period 1979–2016 using the following formula:

$$\mathrm{AAM} = \frac{a^3}{g}\int_{\frac{-\pi}{2}}^{\frac{\pi}{2}}\int_{0}^{2\pi}\int_{\sigma_o}^{\sigma} cos^2\phi \mathrm{d}\phi \mathrm{d}\lambda u \mathrm{d}\sigma, \tag{1}$$

where a is Earth's radius, g is the gravitational constant, ϕ is latitude, λ is longitude, u is zonal wind speed, and σ is the R2 vertical coordinate system. AAM tendency was calculated using a second-order finite difference. AAM and AAM tendency were then used to calculate the GWO (phases 1–8) following a phase diagram used for the MJO (Weickmann & Berry, 2007, 2009; Wheeler & Hendon, 2004).

While GWO phases make for easy climatological classification, they encompass large areas of the AAM and AAM tendency phase space. Thus, 2-D histograms of hail day probability anomaly were calculated and smoothed with a 1σ Gaussian filter to allow for more specific analysis of the relationship between hail and the GWO following:

$$\hat{P}\mathrm{anom}_{i,j} = \hat{P}\mathrm{hailday}_{i,j} - \hat{P}\mathrm{day}_{i,j}, \tag{2}$$

where

$$\hat{P}\mathrm{hailday}_{i,j} = \frac{\mathrm{haildays}_{i,j}}{\sum \mathrm{haildays}_{i,j}} \tag{3}$$

and:

$$\hat{P}\text{day}_{i,j} = \frac{n\text{days}_{i,j}}{\sum n\text{days}_{i,j}}. \quad (4)$$

2.3. NARR

Environmental data from the North American Regional Reanalysis (NARR) on the native 32 km Lambert-conformal grid were drawn for the period 1979–2016 (Mesinger et al., 2006). Thermodynamic pseudosoundings were derived at each grid point using the 3-hourly standard set of 3-D atmospheric variables. Parameters relevant to severe convective storms were then generated, including convective available potential energy, storm relative helicity, and S06. From these parameters, a fixed-layer version of the SCP was calculated and used to evaluate hail environments following previous research (Thompson et al., 2003). SCP was set to zero in the presence of surface-based convective inhibition < -50 J kg^{-1} in attempt to only analyze environments with a limited capping inversion and thus higher probability of thunderstorm initiation. NARR has been shown to underestimate the strength of the capping inversion in the Southern Great Plains, so caution should be used when interpreting visual relationships between positive environmental anomalies and reports in this region (Gensini et al., 2014).

A daily climatology (valid at 2100 UTC) of NARR-derived SCP was created and used to calculate the grid point daily probability of exceeding a SCP value of 1. Daily probability anomalies of SCP exceeding one were calculated, paired to GWO phase and 1800–0000 UTC hail reports, then averaged by corresponding month.

3. Results

3.1. GWO Phase and Hail Reports

Hail frequency depicts a strong relationship to GWO phase (Table 1). To assess significance, probability of a SEV hail day was created (Table 1) and compared to the expected probability for all phases of the respective month. Statistical significance was assessed at the 95% confidence level using a two-tailed binomial test statistic. The GWO plays a significant role in modulating SEV hail day likelihood across all phases during March–May (MAM) and September–November (SON). In June, there is significantly increased probability of SEV hail days in phases 1–3, while no significant decrease in probability is found.

February, July, August, and December show statistical significance only for decreasing likelihood of SEV hail days (during specific phases), and January shows no significance. This broadly suggests that the GWO/SEV hail day relationship is at its strongest during transition seasons and weakest during the winter. During summer, relationships and significance are somewhat mixed, likely owing to SEV hail reports being dominated by mesoscale processes. This seasonal dependence is similar to that found by the MJO (Zhang, 2013) and should be noted by researchers and forecasters. Similar results were found for SIG and GIANT hail reports.

To further visualize this relationship, SEV hail reports were binned by GWO phase, then an efficiency was calculated with units of reports per GWO phase day and expressed as a monthly anomaly (Figure 1). SEV hail reports tend to be favored in GWO phases 1, 2, 3, and 8, whereas SEV hail reports are less likely in GWO phases 4, 5, 6, and 7. Notable exceptions appear in May phase 2, March phase 3, and June phase 4, where −5, −5, and +8 SEV hail reports per GWO phase day anomalies were found, respectively. Annually, the most (least) favored phase for hail frequency is GWO phase 1 (5). Similar results were found for SIG and GIANT hail efficiencies.

3.2. Hail Intensity in Relation to GWO Phase Space

To examine specific AAM and AAM tendency values, 2-D histograms of hail day probability anomaly were created for boreal spring (MAM) and fall (SON) given the statistically significant month-phase results (Table 1). Phase space probabilities do change slightly if further stratified by individual month, but noise increases due to smaller sample sizes with minimal gain in physical interpretation.

For MAM SEV hail days, nearly all amplitudes of GWO phase 8 and 1 are favorable for increased probability of occurrence (Figure 2a). Other phases show a probability dependence based on GWO amplitude (i.e., distance from the origin). For example, SEV hail day probability decreases as GWO amplitude increases in GWO phases 2 and 3, whereas SEV hail day probability increases with GWO amplitude in phase 4. SIG and GIANT hail days (Figures 2b and 2c) reflect similar results, albeit with higher- and lower-magnitude probabilities due to smaller sample sizes.

Table 1
Hail Day Statistics and Likelihood

Phase	Jan	Feb	Mar	Apr	May	Jun	Jul	Aug	Sep	Oct	Nov	Dec
						SEV hail days						
1	15	25	67	102	83	120	95	98	76	38	10	9
2	12	32	67	87	62	143	135	75	82	32	4	3
3	10	18	60	95	66	101	129	76	86	43	8	12
4	8	9	43	59	113	72	88	76	54	29	12	4
5	14	26	35	53	92	60	58	74	33	15	23	7
6	19	44	76	49	82	85	48	81	46	21	8	17
7	18	26	68	69	73	83	68	76	29	25	14	8
8	11	21	66	74	118	85	83	91	37	32	26	10
Neutral	48	56	122	276	420	368	422	420	277	210	81	44
						Total days						
1	120	95	111	119	84	120	99	106	123	85	73	82
2	108	114	121	107	68	144	141	82	116	82	26	59
3	80	90	131	140	69	101	134	82	119	94	81	84
4	92	75	87	80	127	74	82	85	87	101	137	93
5	118	115	82	83	95	61	62	88	56	60	98	83
6	136	140	140	69	86	87	49	88	80	77	57	102
7	107	85	131	98	75	84	71	86	49	59	72	89
8	89	73	108	88	122	88	86	99	65	99	112	109
Neutral	328	287	267	356	452	381	444	462	445	521	484	477
						Average SEV hail reports per phase day						
1	1.0	4.5	19.5	43.4	54.3	39.5	27.0	13.5	8.1	4.1	1.2	1.5
2	0.5	3.2	14.3	36.3	33.8	33.5	22.4	13.9	9.9	4.0	1.9	0.1
3	2.5	2.6	6.2	26.8	55.2	45.7	21.0	11.5	8.5	5.1	0.8	1.2
4	0.7	0.7	13.4	18.8	29.7	41.7	21.0	13.2	5.0	1.8	0.7	0.1
5	0.7	1.9	6.4	12.9	25.4	25.1	14.4	12.4	2.8	0.7	1.2	0.3
6	1.1	3.6	9.4	14.1	28.5	17.7	11.3	8.7	3.8	1.5	0.6	0.9
7	1.2	1.7	8.2	12.5	39.6	27.6	14.2	10.9	6.8	4.5	2.1	0.7
8	1.5	2.2	12.8	35.5	47.8	34.5	19.7	15.2	6.7	1.5	2.7	0.2
Neutral	1.3	1.5	9.6	22.9	33.6	37.4	20.1	13.8	5.1	3.6	1.4	0.6
						Probability anomaly of SEV hail day						
1	0.00	0.01	**0.08**	**0.11**	**0.04**	**0.01**	0.00	0.02	**−0.01**	**0.09**	**−0.02**	0.01
2	−0.01	0.03	**0.03**	**0.07**	**−0.04**	**0.01**	0.00	**0.01**	**0.08**	**0.03**	**−0.01**	**−0.05**
3	0.00	−0.05	**−0.07**	**−0.07**	**0.01**	**0.01**	0.00	0.02	**0.10**	**0.10**	**−0.06**	0.05
4	−0.04	**−0.13**	**−0.03**	**−0.01**	**−0.06**	−0.01	0.00	**−0.01**	0.00	**−0.07**	**−0.07**	**−0.05**
5	−0.01	−0.02	**−0.10**	**−0.11**	**0.02**	0.00	**−0.02**	**−0.06**	**−0.03**	**−0.11**	**0.07**	−0.01
6	0.01	0.06	**0.02**	**−0.04**	0.00	−0.01	0.02	0.02	**−0.05**	**−0.08**	**−0.02**	0.07
7	0.04	0.06	**−0.01**	**−0.04**	**0.02**	0.00	0.00	**−0.02**	**−0.03**	**0.07**	**0.03**	−0.01
8	0.00	0.04	**0.08**	**0.09**	**0.02**	−0.02	0.01	0.02	**−0.05**	**−0.03**	**0.07**	**−0.01**
Neutral	0.02	−0.05	**−0.07**	**0.03**	**−0.02**	**−0.03**	**−0.01**	0.00	0.00	**0.05**	**0.01**	**−0.01**

Note. Based on the period 1979–2016. Bold values indicate a SEV hail day probability anomaly that is significant at the 95% confidence level.

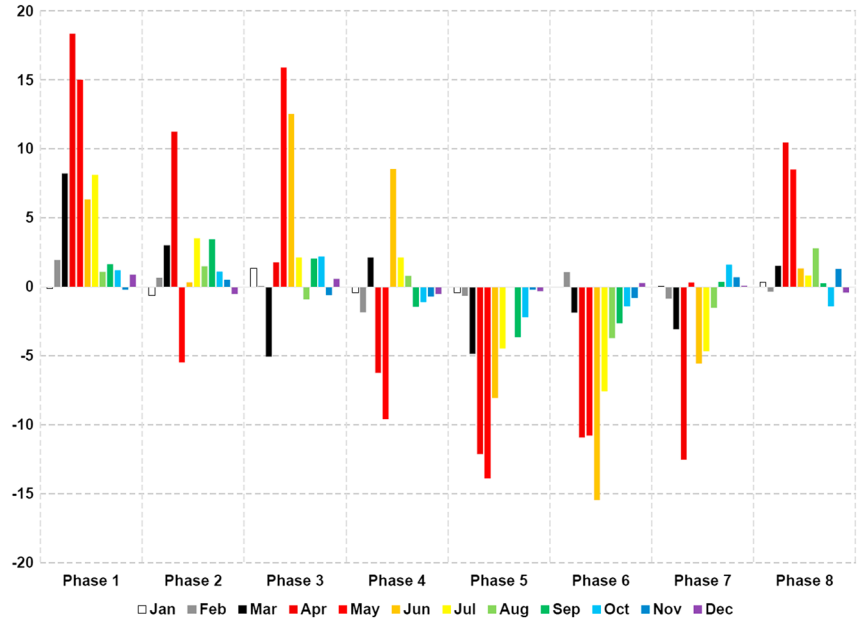

Figure 1. SEV hail report anomaly per Global Wind Oscillation phase day (1979–2016). Report anomalies are calculated based on the monthly average.

Notable differences from MAM SEV and SIG hail day probability anomaly were found when comparing to SON (Figures 2e and 2f). Thus, GWO phase has a seasonal dependence on hail frequency, similar to results found for the MJO (Barrett & Gensini, 2013; Barrett & Henley, 2015). SON exhibits more of a dipole pattern of GWO hail day probability, with higher (lower) frequencies found in low (high) AAM regimes. A small sample size of only 31 events limits any conclusions for GIANT hail in SON (Figure 2g). For both seasons, the changes of SIG and GIANT hail probability reflect a strong modification of atmospheric patterns conducive to the largest hail sizes, which are most likely to cause property damage (Allen et al., 2017).

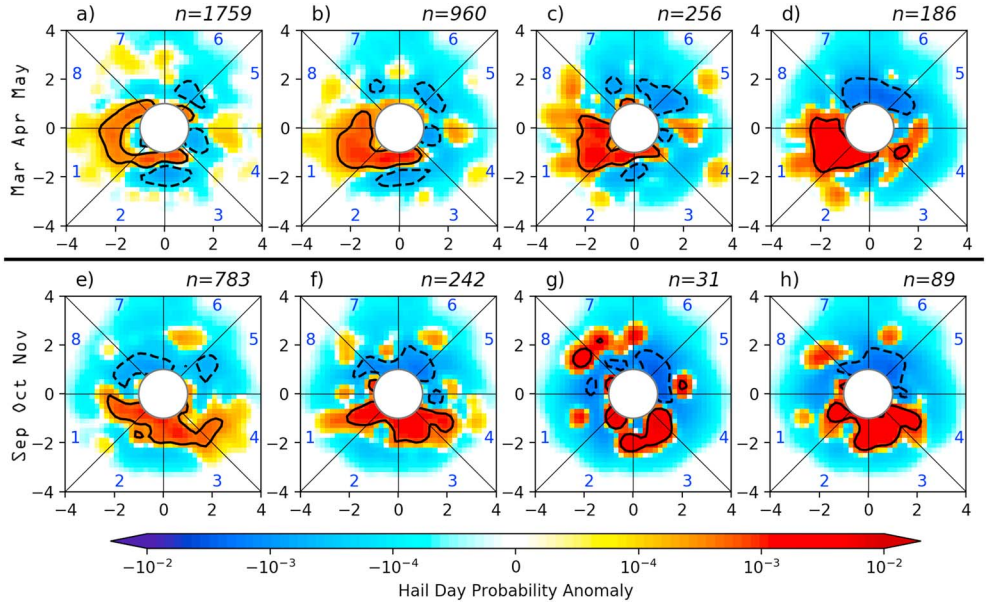

Figure 2. 1979–2016 March–May (MAM) probability anomalies for (a) SEV hail, (b) SIG hail, (c) GIANT hail, (d) 90th percentile SEV hail frequency days and September–November (SON) probability anomalies for (e) SEV hail, (f) SIG hail, (g) GIANT hail, and (h) 90th percentile SEV hail frequency days. Blue numbers indicate the respective Global Wind Oscillation phase, and *n* indicates sample size. Contours indicate significance at the 95% confidence level.

Usually, the largest impacts from hail on society come on days in which widespread damaging hail occurs. These high-frequency days were examined as 90th percentile hail days (>68 SEV reports in a single MAM day, Figure 2d; >24 SEV reports in a single SON day, Figure 2h). Like tornado outbreaks (Gensini & Marinaro, 2015), large SEV hail frequency days are most likely during transition periods to low AAM. However, amplitude of the GWO and seasonality again modulate these results, indicating the importance of examining raw AAM and AAM tendency values in phase space versus simply identifying the categorical GWO phase octave.

3.3. GWO and Hail Environments

Finally, GWO phase and hail day relationship was analyzed using atmospheric environments. This provides corroboration for results found by strictly using reports. In addition, the juxtaposition of environment and report analysis allows for the examination the GWO phase may have on spatial patterns of U.S. hail reports and supercell environments. SCP is used as a proxy for hail environments, specifically focusing on where this calculation is greater than a value of 1, as this has been identified as a statistical discriminator between supercell and nonsupercell environments (Thompson et al., 2003). Furthermore, environmental analysis is restricted to SIG hail days due to a cleaner historical record less likely to be influenced by nonmeteorological factors (Allen & Tippett, 2015; Allen et al., 2017).

Large positive spatial anomalies of the probability of SCP exceeding 1 are found in MAM during GWO phase 1, with the highest values extending from Oklahoma City, OK, to Little Rock, AR, to Louisville, KY (Figure 3a). Many grid point values in this region exceed +0.1, indicating GWO phase 1 increases the probability of a SCP day exceeding 1 by nearly 10%. The positive anomaly of SCP also admirably captures the overall spatial extent of SIG hail reports during this phase, thus increasing confidence in results. MAM phase 2 (Figure 3b) shows an eastward migration of the probability anomalies of SCP, with notable increases in LA, MS, GA, and the Carolinas and decreases in OK, KS, MO, and NE. This is consistent with a conceptual eastward migration of a surface extratropical cyclone. GWO phase 3 begins a transition phase for AAM and shows weaker agreement between SIG hail reports and anomalies of SCP exceeding 1. However, this phase is dependent on GWO amplitude (Figure 2b), suggesting that low-amplitude GWO phase 3 favors increased activity (especially in the Southeast United States), but if the amplitude is >2, SCP environments are less likely across portions of the Central/Southern Great Plains. Ignoring noise, GWO phases 4, 5, and 6 exhibit large spatial areas of negative probabilities of SCP exceeding 1. This is especially true in areas with close proximity to the Gulf of Mexico (5–15% reductions in the grid point probability of SCP exceeding 1). This region of relatively large negative anomalies is significant, as these are climatologically favored areas for the highest SCP values during MAM.

The negative probability anomalies also broadly spatially correlate with a lack of observed SIG hail reports. MAM phases 5, 6, and 7 depict similar results, suggesting that only areas west of longitude 98°W (i.e., the High Plains) have positive anomalies of SCP. In addition, very few SIG hail reports are found east of the Mississippi River in GWO phases 6 and 7 during the month of April. By GWO phase 8, positive probability anomalies (and subsequent large increases in SIG hail reports) return to the Central and Southern Great Plains, Mississippi River Valley, and the Midwest. This marks the return to a period of on-shore flow from the Gulf of Mexico, decreasing static stability, and a more favorable environment for supercell thunderstorms. Spatial maxima in SIG hail reports are generally noted to the west of SCP environmental maxima. This is physically logical given that the SCP only captures the synoptic environment supportive of supercells and does not account for a lifting mechanism (e.g., cold front and dryline) necessary for the initiation of deep convection. Minor differences were found between MAM and SON, mainly with phase 3. In SON, phase 3 was more favorable for supercell environments (and subsequent hail days) versus MAM phase 3. From 500 hPa geopotential and 2 m dew point anomalies, this result is likely associated with a slower eastward wave progression during SON phases 1–3 and consistent with changes in temporal spectral analysis of GWO phase orbits from previous research (Weickmann & Berry, 2007, 2009).

To further corroborate the changes in SCP probabilities with the background synoptic environment, 500 hPa geopotential height, and 2 m dew point anomalies were computed for each phase following the method used for SCP (Figure 4). Phases 8 and 1 depict an anomalously deep thermal trough in the Great Basin and an anomalous ridge positioned in the Mid-Atlantic Region. This would promote southerly surface flow and positive surface dew point anomalies across the majority of the central and eastern United States, supporting the locations of positive SCP anomalies. Dew point anomalies vary by GWO phase as large-scale 500 hPa heights either favor (Figures 4a and 4h) or disfavor (Figures 4d–4f) onshore flow from the Gulf of Mexico.

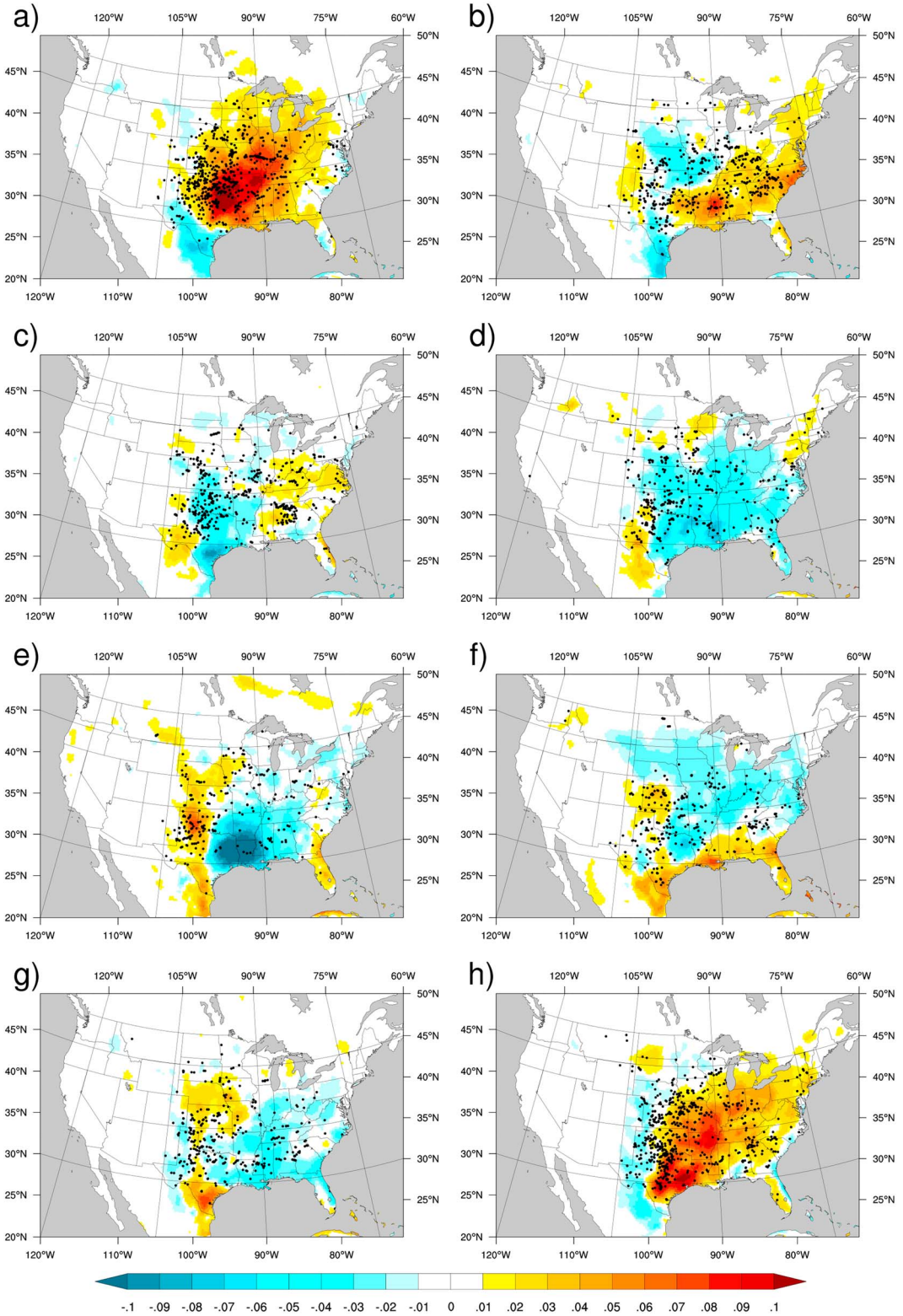

Figure 3. March–May probability anomaly of a supercell composite parameterSCP value exceeding 1 (color fill) for Global Wind Oscillation (a) phase 1, (b) phase 2, (c) phase 3, (d) phase 4, (e) phase 5, (f) phase 6, (g) phase 7, and (h) phase 8 for the period 1979–2016. Black dots indicate reported SIG hail events in the respective Global Wind Oscillation phase.

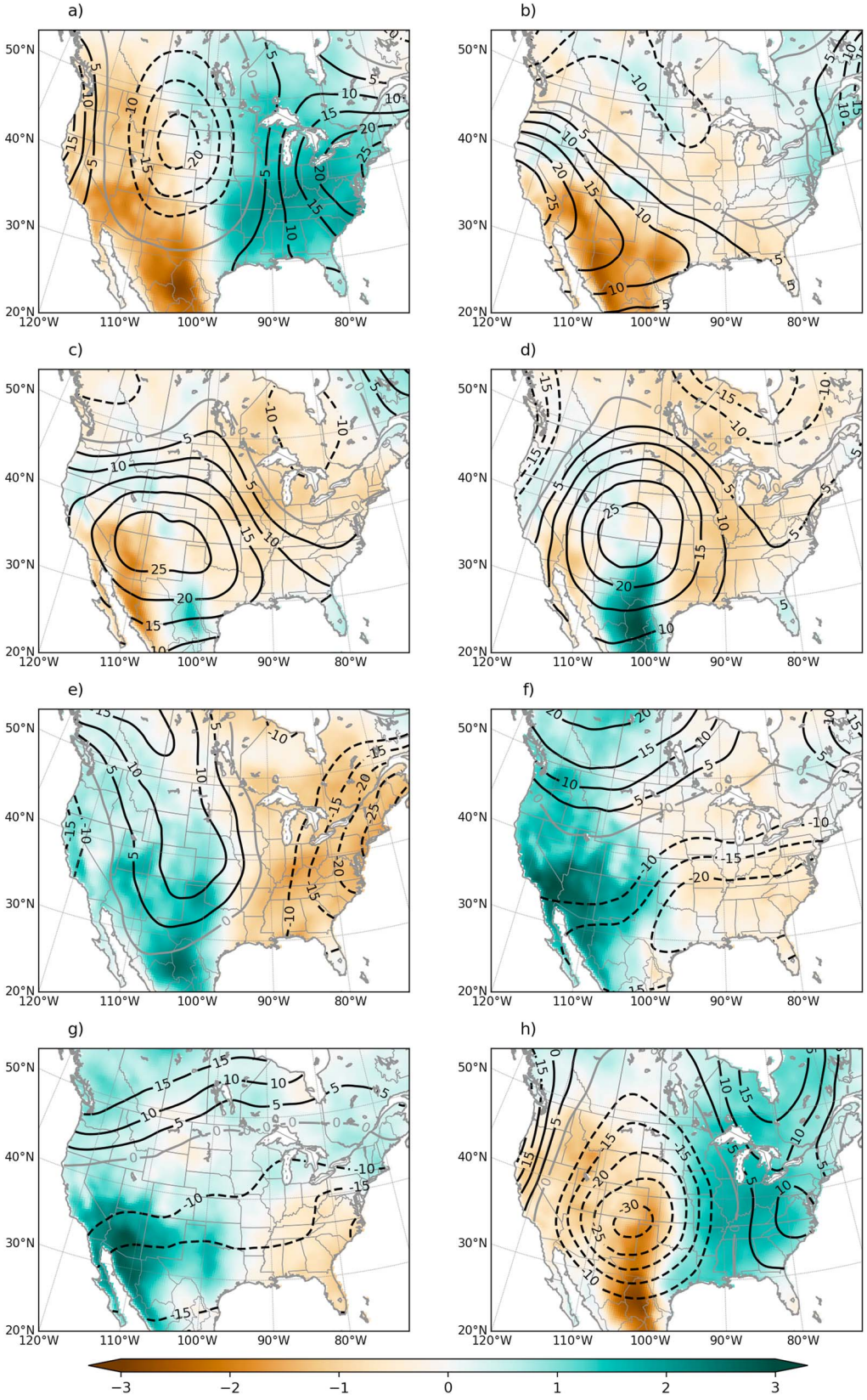

Figure 4. March–May 2 m dew point anomaly (color fill) and 500 hPa geopotential height anomaly (contours) for Global Wind Oscillation (a) phase 1, (b) phase 2, (c) phase 3, (d) phase 4, (e) phase 5, (f) phase 6, (g) phase 7, and (h) phase 8 for the period 1979–2016.

4. Summary and Discussion

Applying the framework of Earth relative AAM using the GWO, it is found that U.S. hail events are more likely to occur during periods of low AAM and less likely in high periods. The strongest relationship between hail and the GWO is found in the spring and fall, reflecting a period when extratropical cyclones and their associated environments produce a majority of hail events. Severe, significant severe, and giant hail events are more likely to occur during GWO phases 8, 1, 2, and 3 during the peak of U.S. severe weather season. In contrast, lower frequencies of hail events are generally found in GWO phases 4, 5, 6, and 7 but vary based on GWO amplitude and specific season. These results are complemented by anomalies of atmospheric ingredients favorable to large hail using the SCP, 500 hPa geopotential height, and 2 m dew point. These results suggest that even with potential nonmeteorological biases in the observations of hail, there is a strong connection between the GWO and U.S. hail frequency. This is similar to the results observed by previous research on tornadoes (Gensini & Marinaro, 2015; Moore, 2017).

Broadly, the GWO is an important metric for describing planetary-scale changes in the global circulation due to tropical convection, extratropical dynamics, and surface torques. These changes modulate jet stream structure, evolution, orientation, and Rossby wave dispersion in the midlatitudes. This modulation leads to changes in the frequency of favorable severe thunderstorm environments as suggested by the analysis herein and prior analysis of tornadoes (Gensini & Marinaro, 2015). A key limitation of this approach occurs in the boreal summer, when GWO has weaker utility for describing variability in supercell environments. Mesoscale processes (e.g., topographic circulations and outflow boundaries) play a dominant role in the initiation and sustenance of severe convection in the summer months (Doswell, 1987), providing a simple physical explanation for the reduced explanatory capability of the GWO. Another potential challenge occurs due to the current framework of calculation for the GWO. The GWO is calculated here as a global integral, rather than on a hemispheric basis, which may lead to confounding results in decomposing relationships to severe weather phenomena when changes in AAM are primarily located in the Southern or Eastern hemisphere. Future work is planned to explore the potential to decompose these (and other) climate signals in order to provide a more robust physical connection between hemispheric teleconnections and severe weather environments. Finally, the relationship demonstrated here also suggests a pathway to prediction of hail frequency at subseasonal forecast leads, as the periodicity of GWO phase orbits is typically between 15 and 80 days (Weickmann & Berry, 2009).

Acknowledgments
The authors declare no funding sources and no conflicts of interest associated with this work. Two anonymous reviewers provided suggestions that improved the quality of this manuscript. Hail reports are available from the storm events database at http://www.spc.noaa.gov/wcm/#data. NARR data were downloaded from the Research Data Archive (RDA) at the National Center for Atmospheric Research (NCAR), Computational and Information Systems Laboratory (CISL) at http://rda.ucar.edu/datasets/ds608.0/. R2 data were also downloaded from the RDA NCAR CISL portal at https://rda.ucar.edu/datasets/ds091.0/.

References

Allen, J. T., & Tippett, M. K. (2015). The characteristics of United States hail reports: 1955–2014. *Electronic Journal of Severe Storms Meteorology*, *10*, 1–31.

Allen, J. T., Tippett, M. K., & Sobel, A. H. (2015). An empirical model relating U.S. monthly hail occurrence to large-scale meteorological environment. *Journal of Advances in Modeling Earth Systems*, *7*, 226–243. https://doi.org/10.1002/2014MS000397

Allen, J. T., Tippett, M. K., & Sobel, A. H. (2015). Influence of the El Niño/Southern Oscillation on tornado and hail frequency in the United States. *Nature Geoscience*, *8*, 278–283.

Allen, J. T., Tippett, M. K., Kaheil, Y., Sobel, A. H., Lepore, C., Nong, S., & Muehlbauer, A. (2017). An extreme value model for United States hail size. *Monthly Weather Review*, *145*, 4501–4519.

Barrett, B. S., & Gensini, V. A. (2013). Variability of central United States April–May tornado day likelihood by phase of the Madden-Julian Oscillation. *Geophysical Research Letters*, *40*, 2790–2795. https://doi.org/10.1002/grl.50522

Barrett, B. S., & Henley, B. N. (2015). Intraseasonal variability of hail in the contiguous United States: Relationship to the Madden–Julian Oscillation. *Monthly Weather Review*, *143*, 1086–1103.

Blair, S. F., Laflin, J. M., Cavanaugh, D. E., Sanders, K. J., Currens, S. R., Pullin, J. I., … Mallinsonn, H. M. (2017). High-resolution hail observations: Implications for NWS warning operations. *Weather and Forecasting*, *32*, 1101–1119.

Cecil, D. J., & Blankenship, C. B. (2012). Toward a global climatology of severe hailstorms as estimated by satellite passive microwave imagers. *Journal of Climate*, *25*, 687–703.

Changnon, S. A. (1977). The scales of hail. *Journal of Applied Meteorology and Climatology*, *16*, 626–648.

Changnon, S. A., & Changnon, D. (2000). Long-term fluctuations in hail incidences in the United States. *Journal of Climate*, *13*, 658–664.

Cintineo, J. L., Smith, T. M., Lakshmanan, V., Brooks, H. E., & Ortega, K. L. (2012). An objective high-resolution hail climatology of the contiguous United States. *Weather and Forecasting*, *27*, 1235–1248.

Computational and Information Systems Laboratory (2000). *NCEP/DOE Reanalysis 2 (r2)*. Boulder CO: Research Data Archive at the National Center for Atmospheric Research, Computational and Information Systems Laboratory. http://rda.ucar.edu/datasets/ds091.0/

Cook, A. R., & Schaefer, J. T. (2008). The relation of El Niño–Southern Oscillation (ENSO) to winter tornado outbreaks. *Monthly Weather Review*, *136*, 3121–3137.

Cook, A. R., Leslie, L. M., Parsons, D. B., & Schaefer, J. T. (2017). The impact of the El Niño Southern Oscillation (ENSO) on winter and early spring U.S. tornado outbreaks. *Journal of Applied Meteorology and Climatology*, *56*, 2455–2478. https://doi.org/10.1175/JAMC-D-16-0249.1

Doswell, C. A., III (1987). The distinction between large-scale and mesoscale contribution to severe convection: A case study example. *Weather and Forecasting*, *2*(1), 3–16.

Doswell, C. A., III, Brooks, H. E., & Kay, M. P. (2005). Climatological estimates of daily local nontornadic severe thunderstorm probability for the United States. *Weather and Forecasting*, *20*, 577–595.
Gensini, V. A., & Marinaro, A. (2015). Tornado frequency in the United States related to global relative angular momentum. *Monthly Weather Review*, *144*, 801–810.
Gensini, V. A., Mote, T. L., & Brooks, H. E. (2014). Severe-thunderstorm reanalysis environments and collocated radiosonde observations. *Journal of Applied Meteorology and Climatology*, *53*, 742–751.
Gunturi, P., & Tippett, M. K. (2017). Managing severe thunderstorm risk: Impact of ENSO on U.S. tornado and hail frequencies (Tech. rep.). WillisRe.
Jung, E., & Kirtman, B. P. (2016). Can we predict seasonal changes in high impact weather in the United States? *Environmental Research Letters*, *11*, 074018.
Kalnay, E., Kanamitsu, M., Kistler, R., Collins, W., Deaven, D., Gandin, L., … Joseph, D. (1996). The NCEP/NCAR 40-year reanalysis project. *Bulletin of the American Meteorological Society*, *77*, 437–471.
Kelly, D. L., Schaefer, J. T., & Doswell, C. A. III (1985). Climatology of nontornadic severe thunderstorm events in the United States. *Monthly Weather Review*, *113*, 1997–2014.
Lee, S.-K., Atlas, R., Enfield, D., Wang, C., & Liu, H. (2012). Is there an optimal ENSO pattern that enhances large-scale atmospheric processes conducive to tornado outbreaks in the United States? *Journal of Climate*, *26*, 1626–1642.
Lee, S.-K., Wittenberg, A. T., Enfield, D. B., Weaver, S. J., Wang, C., & Atlas, R. (2016). US regional tornado outbreaks and their links to spring ENSO phases and North Atlantic SST variability. *Environmental Research Letters*, *11*, 044008.
Lepore, C., Tippett, M. K., & Allen, J. T. (2017). ENSO-based probabilistic forecasts of March–May U.S. tornado and hail activity. *Geophysical Research Letters*, *44*, 9093–9101. https://doi.org/10.1002/2017GL074781
Mesinger, F., DiMego, G., Kalnay, E., Mitchell, K., Shafran, P. C., Ebisuzaki, W., … Coauthors (2006). North American Regional Reanalysis. *Bulletin of the American Meteorological Society*, *87*, 343–360.
Molina, M. J., Timmer, R. P., & Allen, J. T. (2016). Importance of the Gulf of Mexico as a climate driver for U.S. severe thunderstorm activity. *Geophysical Research Letters*, *43*, 12,295–12,304. https://doi.org/10.1002/2016GL071603
Moore, T. W. (2017). Annual and seasonal tornado activity in the united states and the Global Wind Oscillation. *Climate Dynamics*, 1–12. https://doi.org/10.1007/s00382-017-3877-5
Schaefer, J. T., & Edwards, R. (1999). The SPC tornado/severe thunderstorm database. In *Preprints, 11th Conf. applied climatology* (pp. 215–220). Dallas, TX: American Meteor Society.
Thompson, D. B., & Roundy, P. E. (2012). The relationship between the Madden-Julian Oscillation and U.S. violent tornado outbreaks in the spring. *Monthly Weather Review*, *141*, 2087–2095.
Thompson, R. L., Edwards, R., Hart, J. A., Elmore, K. L., & Markowski, P. (2003). Close proximity soundings within supercell environments obtained from the Rapid Update Cycle. *Weather and Forecasting*, *18*, 1243–1261.
Weickmann, K., & Berry, E. (2007). A synoptic–dynamic model of subseasonal atmospheric variability. *Monthly Weather Review*, *135*, 449–474.
Weickmann, K., & Berry, E. (2009). The tropical Madden–Julian Oscillation and the Global Wind Oscillation. *Monthly Weather Review*, *137*, 1601–1614.
Wheeler, M. C., & Hendon, H. H. (2004). An all-season real-time multivariate MJO index: Development of an index for monitoring and prediction. *Monthly Weather Review*, *132*, 1917–1932.
Zhang, C. (2013). Madden–Julian Oscillation: Bridging weather and climate. *Bulletin of the American Meteorological Society*, *94*, 1849–1870.